

Counterfactual Explanations for Land Cover Mapping in a Multi-class Setting

Cassio F. Dantas, Diego Marcos, Dino Ienco

Abstract—Counterfactual explanations are an emerging tool to enhance interpretability of deep learning models. Given a sample, these methods seek to find and display to the user similar samples across the decision boundary. In this paper, we propose a generative adversarial counterfactual approach for satellite image time series in a multi-class setting for the land cover classification task. One of the distinctive features of the proposed approach is the lack of prior assumption on the targeted class for a given counterfactual explanation. This inherent flexibility allows for the discovery of interesting information on the relationship between land cover classes. The other feature consists of encouraging the counterfactual to differ from the original sample only in a small and compact temporal segment. These time-contiguous perturbations allow for a much sparser and, thus, interpretable solution. Furthermore, plausibility/realism of the generated counterfactual explanations is enforced via the proposed adversarial learning strategy.

I. INTRODUCTION

Deep learning techniques have gained widespread popularity in the remote sensing field due to impressive results on a variety of tasks such as image super-resolution, image restoration, biophysical variables estimation and land cover classification from satellite image time series (SITS) data [1]. Of particular importance, this last task provides useful knowledge to support many downstream geospatial analyses [2]. Despite the high performances achieved by recent deep learning frameworks on this task, they remain black-box models with limited understanding on their internal behavior. Due to this limitation, there is a growing need for improving the interpretability of deep learning models in remote sensing with the objective to raise up their acceptability and usefulness, as their decision-making processes are often not transparent [3]–[5]. Counterfactual explanation methods have recently received increasing attention as a means to provide some level of interpretability [6]–[8] to these black-box models. Counterfactual explanations aim to describe the behaviour of a model by providing minimal changes to the input data that would result in realistic samples that result in the model predicting a different class.

For these perturbations to be more easily interpretable it is desirable that they are sparse and that they can be identified with some semantic element of the input data. In the case of time series, this would require to perturb a short and contiguous section of the timeline [9].

Cassio F. Dantas and Dino Ienco are with UMR-TETIS laboratory, INRAE, University of Montpellier, France (email: cassio.fraga-dantas@inrae.fr; dino.ienco@inrae.fr).

Diego Marcos is with Inria, University of Montpellier, France (email: diego.marcos@inria.fr)

Related work: Most papers on counterfactual explanations focus on image data, while much fewer concentrate on time series [9]–[15]. To the best of our knowledge, this is the first paper focusing more specifically on counterfactuals for remote sensing time series data. While [9], [10] also generate time-contiguous perturbations, counterfactual plausibility is achieved by replacing an interval of the time series by a portion of another sample from the dataset [9] or shapelet motifs [10] (also used in [12]). In contrast, we use an adversarial approach to learn a counterfactual generator. In a multivariate setting, the approach in [11] replaces entire variables (not just a time section) with variables from another multivariate sample in the dataset. Related adversarial approaches are proposed in [13], [14], but time localization is not enforced. Finally, in many existing approaches only the binary classification case is considered [10], [14], [15], and when applied to the multi-class case, it usually requires explicitly picking a target class for every counterfactual explanation [11], [13]–[15].

Contributions: Here, we propose a counterfactual generation approach in a multi-class land cover classification setting for satellite image time series data. The proposed approach generates counterfactual explanations that are plausible (i.e. belong as much as possible to the data distribution) and close to the original data (modifying only a limited and contiguous set of time entries by a small amount). Finally, it is not necessary to pre-determine a target class for the generated counterfactual.

Paper outline: In Section II we describe the considered study case with the associated remote sensing data. After detailing the proposed method in Section III, we present the experimental results in Section IV. Concluding remarks and future works are outlined in Section V.

II. STUDY AREA

The study site covers an area around the town of *Koumbia*, in the Province of Tuy, *Hauts-Bassins* region, in the southwest of Burkina Faso. This area has a surface of about 2338 km², and is situated in the sub-humid sudanian zone. The surface is covered mainly by natural savannah (herbaceous and shrubby) and forests, interleaved with a large portion of land (around 35%) used for rainfed agricultural production (mostly smallholder farming). The main crops are cereals (maize, sorghum and millet) and cotton, followed by oleaginous and leguminous crops. Several temporary watercourses constitute the hydrographic network around the city of Koumbia. Figure 1 presents the study site with the reference data (ground truth) superposed on a Sentinel-2 image.

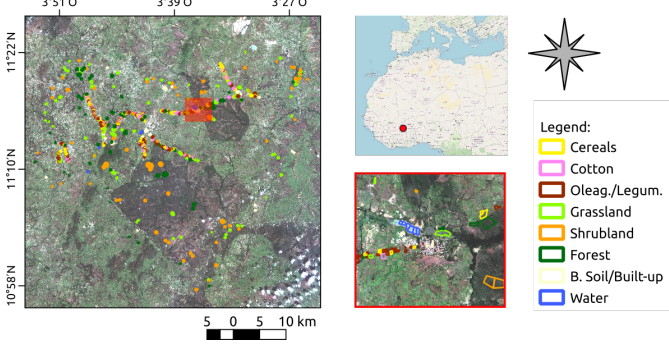


Fig. 1: Location of the *Koumbia* study site. The corresponding ground truth is shown on the right.

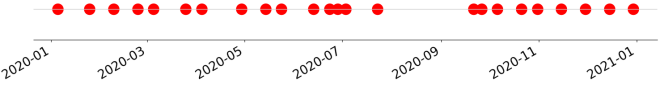


Fig. 2: Acquisition dates of the Sentinel-2 Satellite Image Time Series on the year 2020.

Concerning the satellite data, we collected a time series of Sentinel-2 images spanning the year 2020 from January to December. All images were provided by the THEIA Pole platform¹ at level-2A, which consist of atmospherically corrected surface reflectances (cf. MAJA processing chain [16]) and relative cloud/shadow masks. A standard pre-processing was performed over each band to replace cloudy pixel values as detected by the available cloud masks based on the method proposed in [17]. Figure 2 depicts the acquisition dates of the Sentinel-2 satellite image time series. Finally, from the spectral raw bands at 10-m of spatial resolution the NDVI (Normalized Differential Vegetation Index) was derived.

The GT (ground truth) data for the study site is a collection of (i) digitized plots from a GPS field mission performed in October 2020 and mostly covering classes within cropland and (ii) additional reference plots on non-crop classes obtained by photo-interpretation by an expert. Finally, the polygons have been rasterized at the S2 spatial resolution (10-m), resulting in 79961 labeled pixels. The statistics related to the GT are reported in Table I.

Class	Label	Pixels
1	<i>Cereals</i>	9 731
2	<i>Cotton</i>	6 971
3	<i>Oleaginous</i>	7 950
4	<i>Grassland</i>	12 998
5	<i>Shrubland</i>	22 546
6	<i>Forest</i>	17 435
7	<i>Bare Soil/Built-up</i>	1 125
8	<i>Water</i>	1 205
Total		79 961

TABLE I: *Koumbia* study site Ground Truth statistics.

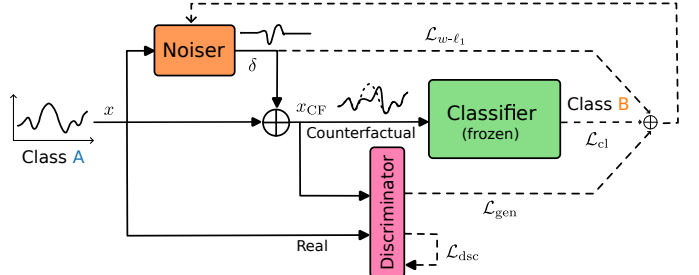


Fig. 3: Schematic representation of the proposed approach.

III. PROPOSED METHOD

A. Architecture overview

For the counterfactual generation, we propose a GAN (generative adversarial network) inspired architecture which is summarized in Fig. 3.

A counterfactual x_{CF} is obtained for each input sample x by adding a perturbation δ to the original signal:

$$x_{CF} = x + \delta \quad (1)$$

The perturbation δ is generated by a *Noiser* module which is learned with the goal to swap the prediction of the *Classifier*. Finally, a *Discriminator* module is leveraged to ensure the generation of realistic counterfactual examples.

B. Networks implementation and training

Regarding the different components on which our framework is built on, we get inspiration by state of the art literature in the field of satellite image time series land cover mapping. For the *Classifier* network we leverage the Temporal Convolutional Neural Network (TempCNN) model proposed in [18]. This architecture has an encoder based on several one-dimensional convolutional layers to explicitly cope with the temporal dimension of the time series data followed by two fully connected layers and a final output layer to provide the multi-class decision.

For the *Discriminator* network we adopt the same architecture as the *Classifier* network and we replace the output layer with a single neuron with sigmoid activation function as commonly done for discriminator networks in adversarial learning [19].

Concerning the *Noiser* module, it is implemented as a multi-layer perceptron network with two hidden layers (each with 128 neurons) and an output layer with the same dimensionality of the time series data. For each of the hidden layers, batch normalization, tangent activation function and a drop-out regularization are employed in this order while for the output layer only the tangent activation function is used. The tangent activation function allows us to restrict the output domain between -1 and +1 thus, facilitating the learning process of the different networks.

The *Classifier* model is pre-trained on the training set and, successively, frozen during the adversarial learning stage since this stage is devoted to learn the model weights associated to the *Noiser* and the *Discriminator* (see section III-D).

¹<http://theia.cnes.fr>

The *Noiser* module is updated with respect to a composite loss made of three parts detailed in sections III-C to III-E.

$$\mathcal{L}_{\text{noiser}} = \mathcal{L}_{\text{cl}} + \lambda_{\text{gen}} \mathcal{L}_{\text{gen}} + \lambda_{w-\ell_1} \mathcal{L}_{w-\ell_1} \quad (2)$$

C. Class-swapping loss

To generate counterfactuals that effectively change the predicted class for a given input we use the following loss:

$$\mathcal{L}_{\text{cl}} = -\frac{1}{n} \sum_{i=1}^n y^{(i)} \log(1 - p(y^{(i)})) \quad (3)$$

It enforces the reduction of the classifier's softmax output for the original label $y^{(i)}$, here denoted $p(y^{(i)})$, eventually leading to a change on the predicted class.

Note that, conversely to standard literature [13], [15] in which a target class for the counterfactual example is chosen a priori, here we purposely do not enforce the prediction of a predefined target class. Instead, we let the *Noiser* free to generate a perturbation δ that will change the classifier output to any other class different from y_i .

D. GAN-based regularization for plausibility

Counterfactual plausibility is enforced via a GAN-inspired architecture, where a discriminator is trained to identify unrealistic counterfactuals while, simultaneously, the *Noiser* module acts as a generator with the goal to fool the discriminator in a two player game.

The *Discriminator* is updated with respect to a standard GAN loss classifying real versus fake (counterfactual) samples:

$$\mathcal{L}_{\text{dsc}} = -\frac{1}{n} \sum_{i=1}^n \left[\log D(x^{(i)}) + \log \left(1 - D(x_{\text{CF}}^{(i)}) \right) \right] \quad (4)$$

where $D(x^{(i)})$ denotes the discriminator's output for a real input $x^{(i)}$ (with expected output 1) and $D(x_{\text{CF}}^{(i)})$ its output for a fake input $x_{\text{CF}}^{(i)}$ (with expected output 0).

The following non-saturating generator loss is used in the *Noiser* update:

$$\mathcal{L}_{\text{gen}} = -\frac{1}{n} \sum_{i=1}^n \log \left(D(x_{\text{CF}}^{(i)}) \right) \quad (5)$$

\mathcal{L}_{gen} is minimized when the discriminator wrongly identifies the counterfactuals as real inputs.

E. Unimodal regularization for time-contiguity

To generate perturbations concentrated around a contiguous time frame we employ a weighted L1-norm penalization, with weights growing quadratically around a central time $\tilde{t}^{(i)}$ chosen independently for each sample $i \in \{1, \dots, n\}$:

$$\mathcal{L}_{w-\ell_1} = \frac{1}{n} \sum_{i=1}^n \sum_{t=1}^T d(t, \tilde{t}^{(i)})^2 |\delta_t^{(i)}| \quad (6)$$

where, for the i -th sample, $\tilde{t}^{(i)}$ is chosen as the time step with the highest absolute value perturbation $\tilde{t}^{(i)} = \text{argmax}_t |\delta_t^{(i)}|$.

To avoid biasing \tilde{t} towards the center, we use the modulo distance $d(t, \tilde{t}) = \min((t - \tilde{t})\%T, (\tilde{t} - t)\%T)$ which treats the time samples as a circular list.

This regularization also brings a degree of sparsity to the generated perturbation δ , since its entries will tend to vanish when getting far away from \tilde{t} . Finally, penalizing the entries of δ enforces the proximity (similarity) between x_{CF} and x .

IV. RESULTS

In this section we inspect the behaviour of the proposed method considering the study case introduced in Section II. More precisely, we first provide a general analysis of the class transitions induced by the counterfactual generation process. Secondly, we discuss per-class average perturbations generated by our framework as well as specific counterfactual examples. Then, we assess the plausibility of the generated counterfactual examples via anomaly detection strategies as suggested in [15]. Finally, we perform an ablation analysis to assess the role of the different loss functions involved in the learning process of our framework.

A. Experimental setup

The *Koumbia* study case described in Section II was split into training, validation and test sets containing respectively 50-17-33% of the 79961 samples. Each data sample corresponds to a (univariate) NDVI time series with 24 time samples (cf. Fig. 2).

First, the *Classifier* was trained over 1000 epochs with batch size 32 and Adam optimizer with learning rate 10^{-4} and weight decay of same value. The model weights corresponding to the best obtained F1-score on the validation set were kept.

Then, with the classifier weights frozen, the *Noiser* and *Discriminator* modules are simultaneously trained over 100 epochs with batch size 128 and Adam optimizer.

Regularization parameters: we set $\lambda_{\text{gen}} = 5 \cdot 10^{-1}$ and $\lambda_{w-\ell_1} = 5 \cdot 10^{-2}$ on the reported results. In practice, increasing these weights implies in further constraining the set of admissible perturbations which, in turn, leads to a smaller rate of successful counterfactual samples –i.e., those that actually change the classifier's prediction (see details in section IV-E). The chosen values lead to a success rate of about 50%. Naturally, by further relaxing these constraints (reducing λ_{gen} and $\lambda_{w-\ell_1}$) would lead to higher success rates, but the generated counterfactual samples would be of lesser quality in terms of plausibility (due to λ_{gen}) as well as time localization and proximity (due to $\lambda_{w-\ell_1}$).

B. Visualizing class relationships

The class transitions induced by the counterfactual samples are summarized in Fig. 4. The left (resp. right) graph was generated by feeding the obtained network with each of the training (resp. test) data samples. They present very similar behavior, which attests the fact that the proposed method generalizes well to previously unseen data. We recall that the class transitions are to no extent pre-defined on our approach; on the contrary, our method allows input samples from the

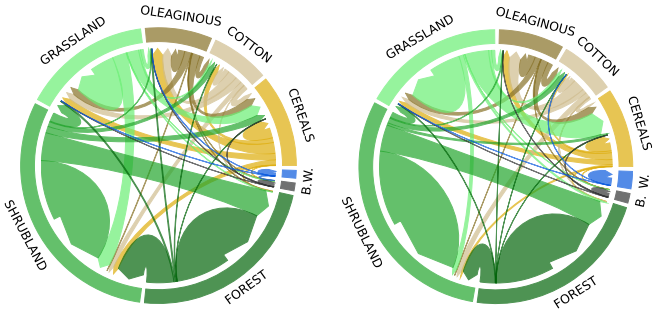


Fig. 4: Summary of class transitions induced by the counterfactuals. Training data (left) and test data (right), where B. stands for *Bare Soil* and W. for *Water* classes.

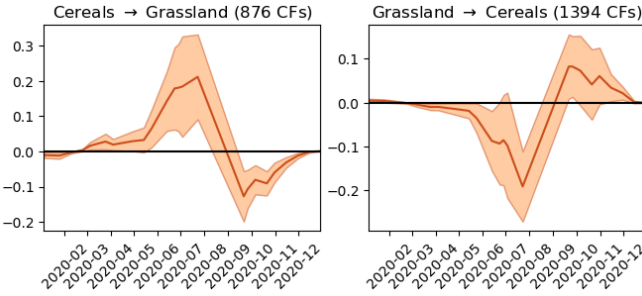


Fig. 5: Examples of average counterfactual perturbations between classes *Cereals* and *Grassland* on both ways. Shaded area corresponds to the standard deviation.

same class to freely split-up into multiple target classes. Transitions obtained in such a way thus bring up valuable insights on the relation between classes.

The obtained transitions are very much in line with the intuitive relation between the different classes. For instance, the three crop-related classes (*Cereals*, *Cotton* and *Oleaginous*) form a very coherent cluster, with almost all transitions staying within the sub-group. The vegetation classes *Shrubland* and *Forest* are most often sent to one another, while *Grassland* remains much closer to the crop classes (especially *Oleaginous*). The *Bare Soil* class is also most often transformed into *Oleaginous*. Finally, the *Water* class is very rarely modified by the counterfactual learning process, which is somewhat expected due to its very distinct characteristic (NDVI signature) compared to the other classes.

The ratio of successful class-swapping counterfactual samples –i.e., those that actually change the classifier’s prediction– was 52.7% (17947 over 34066) for the training data and 43.8% (8765 over 20006) for the test data, considering only the samples that were correctly classified before counterfactuals.

C. Counterfactual examples

Examples of average perturbation profiles for two different class transitions are depicted in Fig 5.

It is interesting to notice how the perturbations correspond roughly to the opposite of each other, which is quite suitable since they correspond to opposite transitions between the same two classes.

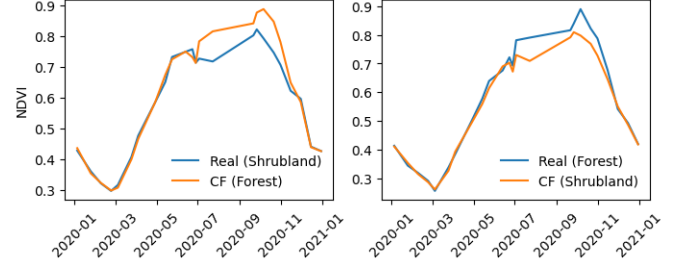


Fig. 6: Examples of original time series with corresponding counterfactual from classes *Shrubland* (4) and *Forest* (5) on both ways.

Two illustrative examples of counterfactual explanations are shown in Fig. 6. It is interesting to observe the similarity between the generated counterfactual and a real data example from the same class (on the neighboring plot).

To transform a *Shrubland* sample into a *Forest* one, NDVI is added between the months of July and October. The opposite is done to obtain the reverse transition, which matches the general knowledge of such land cover classes on the considered study area. Also note that the NDVI peak is slightly shifted from one class to another.

From the provided examples, one can verify that the obtained counterfactual do look realistic (this aspect is further evaluated in section IV-D) besides differing from the real signal only on a contiguous time window. These two properties have been explicitly enforced via the losses in eqs. (5) and (6).

D. Plausibility analysis

In this section, we quantify to what extent the proposed counterfactual explanations fit the original data distribution. To do so, we run an anomaly detection method, Isolation Forest [20], on both the original data and corresponding counterfactuals. To attest the importance of the proposed adversarial training for the generation of realistic/plausible counterfactuals, we perform an ablation study confronting the proposed model trained with and without the generator loss in Eq. (5). Fig. 7 shows contingency matrices relating the isolation forest outputs on the original data (rows) and on the corresponding counterfactual explanations (columns). Two counterfactual generation approaches are investigated: the proposed method (left matrix) and its non-adversarial variant (right matrix). In the figures, diagonal entries correspond to matching isolation forest outputs –i.e., same prediction (inlier/outlier) for both real and counterfactual data. Later, in Table II we compute some metrics on such contingency matrices to further quantify and summarize the behaviour of the compared methods. The proposed counterfactual model achieves impressive results, even leading to more samples identified as inliers than the real data itself (23806 against 23755), since proposed approach converts less inliers into outliers (164) than the other way around (215).

The non-adversarial variant, on the other hand, obtains considerably more degraded results, as it converts as many as 4338 real inlier samples into outliers (about 20 times more). Such a gap becomes evident when looking at the

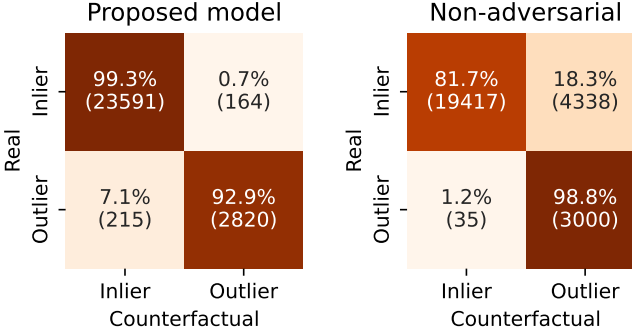


Fig. 7: Isolation forest results on real (rows) and counterfactual data (columns). Proposed model with (left) and without (right) adversarial loss during training. Row-normalized percentages.

corresponding accuracy and normalized mutual information (NMI) computed w.r.t. the isolation forest results on the original data (cf. Table II). Such scores measure to what degree the inlier/outlier partitioning obtained on the counterfactual samples (for each of the two compared variants) matches the one obtained on the original data. The higher they are the better the two partitions match. The obtained results clearly show that counterfactual plausibility is achieved thanks to the adversarial training process.

Method	Accuracy	NMI	Inliers ratio
Proposed	98.6%	0.808	88.9%
Non-adversarial	83.7%	0.337	72.6%

TABLE II: Plausibility analysis using different performance metrics. Isolation Forest results on the real data were used as ground truth for the accuracy and NMI scores.

E. Other ablation studies

In Table III we compare the number of successful class-swapping counterfactual samples as well as the average ℓ_2 and ℓ_1 norms of the perturbations δ generated by the proposed model and two variants ignoring the generator loss (\mathcal{L}_{gen}) and the weighted- ℓ_1 loss ($\mathcal{L}_{w-\ell_1}$), respectively.

One can see that the removal of the auxiliary losses significantly bumps the class-swapping rate, but it happens at the expense of either: 1) counterfactual plausibility, as shown in the Section IV-D for the removal of \mathcal{L}_{gen} ; 2) counterfactual proximity/similarity, as demonstrated by the dramatic increase on the norm of the generated perturbations (or, equivalently, the distance between x and x_{CF}) upon removal of $\mathcal{L}_{w-\ell_1}$.

Method	Class-swap CF	Average $\ \delta\ _2$	Average $\ \delta\ _1$
Proposed	43.8%	0.24 ± 0.18	0.76 ± 0.54
Without \mathcal{L}_{gen}	83.7%	0.97 ± 0.47	1.69 ± 0.99
Without $\mathcal{L}_{w-\ell_1}$	99.6%	4.79 ± 0.07	23.3 ± 0.53

TABLE III: Ablation study on test data.

V. CONCLUSION

In this letter we have presented a new framework to generate counterfactual SITS samples of vegetation indices (i.e. NDVI)

for the land cover classification task. The proposed method overcomes the restriction to apriori define the source and the target classes for the counterfactual generation process while it exploits adversarial learning to ensure realistic counterfactual samples. As possible future work, we would extend the framework to the case of multivariate time series satellite data as well as leverage the feedback provided by the generated counterfactual samples to improve the robustness of the land cover classifier regarding the most frequent class confusions.

REFERENCES

- [1] Q. Yuan, H. Shen, T. Li, Z. Li, S. Li, Y. Jiang, H. Xu, W. Tan, Q. Yang, J. Wang, J. Gao, and L. Zhang, “Deep learning in environmental remote sensing: Achievements and challenges,” *Remote Sensing of Environment*, vol. 241, p. 111716, 2020.
- [2] J. Inglada, A. Vincent, M. Arias, B. Tardy, D. Morin, and I. Rodes, “Operational high resolution land cover map production at the country scale using satellite image time series,” *Remote. Sens.*, vol. 9, no. 1, p. 95, 2017.
- [3] A. Adadi and M. Berrada, “Peeking inside the black-box: a survey on explainable artificial intelligence (XAI),” *IEEE access*, vol. 6, 2018.
- [4] R. Guidotti, A. Monreale, S. Ruggieri, F. Turini, F. Giannotti, and D. Pedreschi, “A survey of methods for explaining black box models,” *ACM Comput. Surv.*, vol. 51, no. 5, Sep. 2019.
- [5] A. B. Arrieta, N. Díaz-Rodríguez, J. Del Ser, A. Bennetot, S. Tabik, A. Barbado, S. García, S. Gil-López, D. Molina, R. Benjamins *et al.*, “Explainable Artificial Intelligence (XAI): Concepts, taxonomies, opportunities and challenges toward responsible AI,” *Information fusion*, vol. 58, pp. 82–115, 2020.
- [6] S. Wachter, B. Mittelstadt, and C. Russell, “Counterfactual explanations without opening the black box: Automated decisions and the gdpr,” *Harv. JL & Tech.*, vol. 31, p. 841, 2017.
- [7] S. Verma, J. Dickerson, and K. Hines, “Counterfactual explanations for machine learning: A review,” *arXiv preprint arXiv:2010.10596*, 2020.
- [8] R. Guidotti, “Counterfactual explanations and how to find them: literature review and benchmarking,” *Data Mining and Knowledge Discovery*, pp. 1–55, 2022.
- [9] E. Delaney, D. Greene, and M. T. Keane, “Instance-based counterfactual explanations for time series classification,” in *International Conference on Case-Based Reasoning*. Springer, 2021, pp. 32–47.
- [10] P. Li, S. F. Boubrahimi, and S. M. Hamdi, “Motif-guided time series counterfactual explanations,” *arXiv preprint arXiv:2211.04411*, 2022.
- [11] E. Ates, B. Aksar, V. J. Leung, and A. K. Coskun, “Counterfactual explanations for multivariate time series,” in *International Conference on Applied Artificial Intelligence (ICAPAI)*, 2021, pp. 1–8.
- [12] R. Guidotti, A. Monreale, F. Spinnato, D. Pedreschi, and F. Giannotti, “Explaining any time series classifier,” in *IEEE International Conference on Cognitive Machine Intelligence (CogMI)*, 2020, pp. 167–176.
- [13] J. Lang, M. Giese, W. Ilg, and S. Otte, “Generating sparse counterfactual explanations for multivariate time series,” *arXiv preprint arXiv:2206.00931*, 2022.
- [14] A. Van Looveren, J. Klaise, G. Vacanti, and O. Cobb, “Conditional generative models for counterfactual explanations,” *arXiv preprint arXiv:2101.10123*, 2021.
- [15] S. Filali Boubrahimi and S. M. Hamdi, “On the mining of time series data counterfactual explanations using barycenters,” in *ACM CIKM*. ACM, 2022, p. 3943–3947.
- [16] O. Hagolle, M. Huc, D. Villa Pascual, and G. Dedieu, “A multi-temporal and multi-spectral method to estimate aerosol optical thickness over land, for the atmospheric correction of formosat-2, landsat, venus and sentinel-2 images,” *Rem. Sens.*, vol. 7, no. 3, pp. 2668–2691, 2015.
- [17] J. Inglada, A. Vincent, M. Arias, and B. Tardy, “iota2-a25386,” Jul. 2016. [Online]. Available: <https://doi.org/10.5281/zenodo.58150>
- [18] C. Pelletier, G. I. Webb, and F. Petitjean, “Temporal convolutional neural network for the classification of satellite image time series,” *Remote. Sens.*, vol. 11, no. 5, p. 523, 2019.
- [19] A. Creswell, T. White, V. Dumoulin, K. Arulkumaran, B. Sengupta, and A. A. Bharath, “Generative adversarial networks: An overview,” *IEEE Signal Process. Mag.*, vol. 35, no. 1, pp. 53–65, 2018.
- [20] O. Li, H. Liu, C. Chen, and C. Rudin, “Deep learning for case-based reasoning through prototypes: A neural network that explains its predictions,” *AAAI Conference on Artificial Intelligence*, vol. 32, no. 1, Apr. 2018.